P36

Cheap robust sensing for obstacle avoidance navigation inspired by echolocation behavior of bats

Yasufumi Yamada*, Kentaro Ito**, Ryo Kobayashi**, ***, Shizuko Hiryu*
*Faculty of Life and Medical Sciences, Doshisha University, Japan
yasufumi.yamada1@gmail.com
**Department of Mathematical and Life Sciences, Hiroshima University, Japan
***Japan Science and Technology Agency, CREST, Japan

1 Introduction

Bats possess a highly developed biosonar system (echolocation[1]) that can be regarded as the minimum sensor requirement (one transmitter and two receivers) for three-dimensional spatial sensing. Despite this, bats can realize robust navigation in a complex environment. The present study 1) experimentally investigated changes in the pulse direction, pulse emission timing and flight path of *Rhinolophus ferrumequinum nippon* during an obstacle avoidance flight as the bats became familiar with the space around them and 2) expressed behavioral principles observed in the bats during flight using an algorithm and then embedded the principles into an autonomous vehicle equipped with simple ultrasound sensors.

2 Obstacle avoidance flight of bats

2.1 Subjects, Materials and Methods

Three adult Japanese horseshoe bats (*Rhinolophus ferrumequinum nippon*) were used. Figure 1*b* shows a top view of the measurement system. Twelve continuous repeated flights of bats were observed to compare the echolocation behaviors between unfamiliar and familiar spaces. The 3D flight path of the bats was recorded using two digital high-speed video cameras (MotionPro X3; IDT Japan, Tokyo, Japan [125 fps]). Echolocation sounds emitted by flying bats were recorded using a custom-made telemetry microphone (Telemike : [2]) which was attached to the back of the bat. In addition, 20-ch microphone array was set up in the walls surrounding the chamber to measure the horizontal pulse direction [3]. For each emitted sound, the sound pressure levels of each microphone within the array were converted into vectors, and the pattern of pulse directivity was fitted to a Gaussian function for the sound pressure vectors across all microphones. Then, the pulse direction was determined at the peak direction of the reconstructed pulse directivity pattern (Figure 1c). Sound recording was synchronized with video recordings by using external trigger.

2.2 Pulse direction control behavior of bats

All three bats reduce the curvature of flight turn with increasing the average flight speed (2.7–3.0 m/s in the 1st trial, 3.2–3.8 m/s in the 12th trial) as the bat repeated the flight. At the same time, pulse emissions from the three bats were reduced to 55% from the first to the last of the 12 flight. Figure 2a and b shows the representative flight path and pulse direction of bats during 1st and 12th flights. The bats shifted the pulse direction dynamically relative to their flight direction in the 1st flight (Figure 2*a*). More precisely, some emissions were aimed directly around each edge of

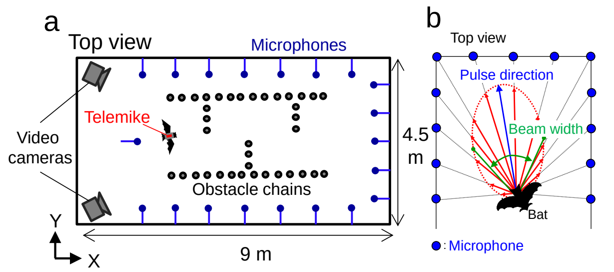

Figure 1: (*a*) Arrangement of the microphone array and chain of obstacles in the flight chamber. (*b*) Calculation procedure of the horizontal pulse direction and beam width using the microphone array.

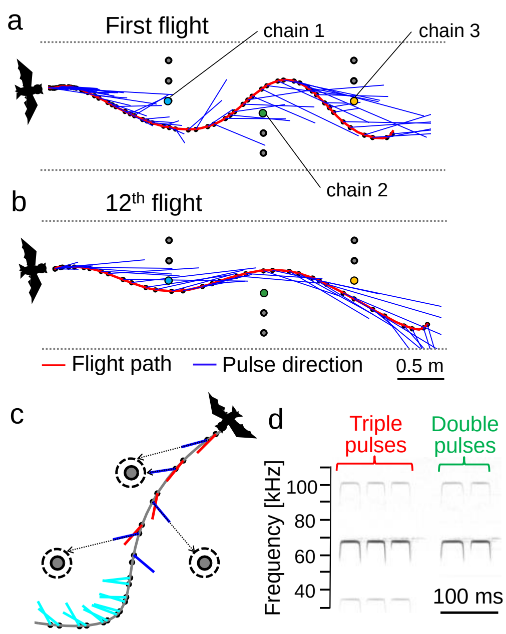

Figure 2: Top views of flight trajectory (red line) and pulse direction (blue line) during the 1st (*a*) and 12th flights (*b*) in the obstacle course. (*c*) Examples of pulse direction control by the bats during unfamiliar space flight in the various obstacle environments. (*d*) Sonograms of typical pulse emission sequences in *R. ferrumequinum nippon* during flight.

the three obstacle chain arrays during the 1st flight. In contrast, the pulse direction was shifted smoothly and directed towards the intended flight direction in the 12th flight trial (Figure 2b). These findings demonstrated that acoustic gaze and flight path controls in bats differ between flights in unfamiliar and those in familiar spaces, suggesting that the bats could characterize their obstacle environment by echolocation and adapt their acoustic gaze control for their own flight path.

Especially, while bats fly in an unfamiliar space, the direction of pulse emission was alternatively shifted between the intended flight direction and the nearby obstacle direction with double or triple pulses (Figure 2c and d), which has very often observed in any layouts and any individuals, appears to be a behavioral principle of bats during flight in unfamiliar space.

3 Demonstration of navigation algorithm inspired by bats

3.1 Double pulse scanning algorithm inspired by bats

In this study, double-pulse scanning (DPS) system was proposed as a bat-inspired navigation algorithm in which 1) the direction of pulse emission was alternately shifted between the direction of movement and the direction of the nearest obstacle, and 2) the direction of movement was calculated for every double-pulse emission based on integrated information from all echoes detected by double-pulse sensing (Figure 3a). To quantify the double-pulse scanning system, a conventional scanning system was also developed, in which 1) the pulse direction was fixed to current moving on-axis, and 2) the moving direction was calculated for every pulse emission.

We constructed an obstacle-avoidance model for both the conventional and double-pulse scanning systems to control the vehicle's moving direction using multiple obstacle information (MOA model). To explain the MOA model briefly, we determined the moving direction φ_d in the case of the conventional scanning system using the following equation (Figure 3b):

$$\varphi_d(t_{i+1}) = \arg(e^{i\varphi_d(t_i)} - 2\sum_{n=1}^{N(t_i)} \sqrt{\frac{\alpha}{r(t_i,n)}} \sin\left(\arctan\frac{k}{r(t_i,n)}\right) e^{i\theta(t_i,n)}) \quad (1)$$

where α = 0.015625 m, k = 1.3 m, $N(t_i)$ indicates number of all obstacles detected by the i^{th} pulse emission. The moving direction φ_d was changed after the i^{th} pulse emission. In contrast, in the case of DPS system, after the 2nd pulse emission of the j^{th} double pulse, φ_d could be determined using the following equation(Figure 3a):

$$\varphi_d(t_{j+1}^{1st})$$

$$= \arg(e^{i\varphi_d(t_j^{1st})} - 2\sum_{n=1}^{N(t_j^{1st})} \sqrt{\frac{\alpha}{r(t_j^{1st},n)}} \sin\left(\arctan\frac{k}{r(t_j^{1st},n)}\right) e^{i\theta(t_j^{1st},n)}$$

$$- 2\sum_{n=1}^{N(t_j^{2nd})} \sqrt{\frac{\alpha}{r(t_j^{2nd},n)}} \sin\left(\arctan\frac{k}{r(t_j^{2nd},n)}\right) e^{i\theta(t_j^{2nd},n)} \quad (2)$$

where α = 0.0078125 m, and k = 1.3 m. Thus, the moving direction φ_d in the double-pulse scanning system was calculated using all obstacle information obtained from the 1st and the 2nd pulse emissions.

3.2 Vehicle design and experiment setting

Vehicle equipped one transmitter (MA40S4R; Murata, Kyoto, Japan), two receivers (SPM0404UD5; Knowles, Itasca, IL, USA) and a central processing unit (Arduino LLC, Somerville, MA, USA). The pulse direction could be adjusted independently of the control of the vehicle driving direction by attaching servomotor under the sensor units. The transmitted ultrasound was 40 kHz (2 ms in duration) and extract echo arrival timings for all echoes detected within 30 ms at the time of pulse emission. The distance from the vehicle to the object r and the direction toward to the object θ were calculated by time differences between pulse and echo and between the right and left received echo. Inter-pulse moving distance (IPD) of the vehicle was set as 13 cm, which was same as average IPD of the bats during flight. DPS system and conventional system were tested100 times in obstacle course, respectively. Initial 10 trials of each system were also recorded vehicle driving path, pulse direction and calculated obstacle localization

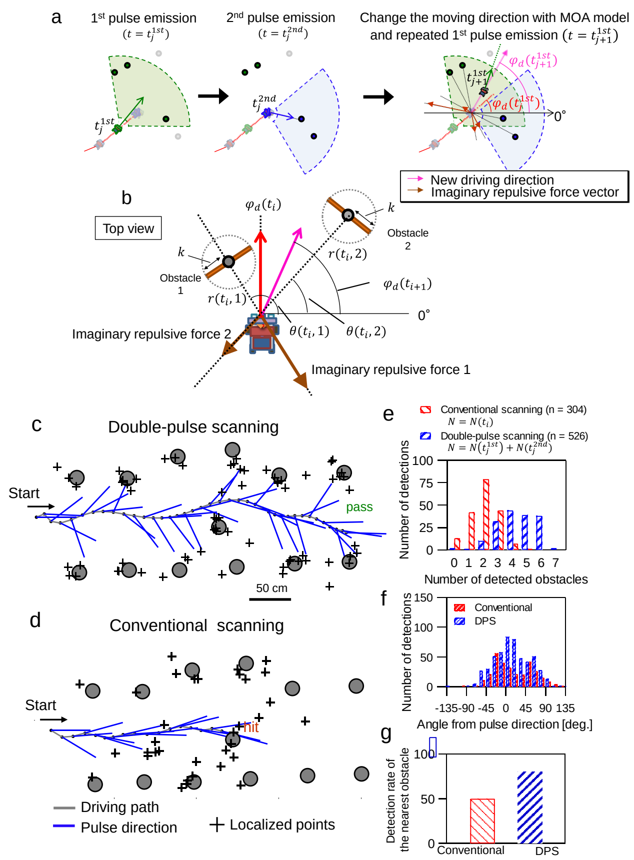

Figure 3: (*a*) Schematic of control law for pulse direction φ_p in the double-pulse scanning system. (*b*) Top view of the schematics of the MOA model. Top views of representative driving trajectories and pulse directions for the double-pulse scanning system (*c*) and the conventional scanning system (*d*). All obstacle positions localized by the vehicle are shown with cross marks. Distributions of the number of obstacles N that were used to calculate moving direction (*e*) and obstacle-detection angle from the pulse direction (*f*) in each system. (*g*) Comparison of detection rates of the nearest obstacles, according to vehicle coordination, between the conventional and double-pulse scanning systems.

3.3 Demonstration results and discussion

The total success rates for the 100 obstacle-avoidance drive trials on this course were 13% for the conventional system and 73% for the DPS system. The localized positions of each system (figure 3c and d), however, deviated from the actual obstacle positions, which was non-significant difference (Mann–Whitney U-test, P = 0.07) suggesting that localization accuracy for detected obstacles is not a critical factor in obstacle-avoidance performance vehicles using conventional compared with double-pulse scanning systems.

For avoidance calculation, 1) DPS system had acquired information of obstacles twice as much as the conventional system by double sensing (figure 3e). In addition, DPS system tended to 2) detect obstacles around the centre of the pulse's own acoustic field (Figure 3f) 3) without losing the nearest obstacle by alternate shifting the pulse direction toward obstacle direction and ahead of moving direction (Figure 3g).

Our findings suggest that the integration of information from two emissions is effective; i.e. acoustic sight restricted to only one transmitter and two receivers, demonstrating that the ingenuity inspired by animals exerts a large effect in simple design sensing.

References

[1] J.D. Altringham, "Bats: biology and behavior", vol. 262, 1996.
[2] Hiryu et al., J. Acoust. Soc. Am., vol.118, 3927-3933, 2005.
[3] Matsuta. Et .al.,J. Exp. Biol., vol. 216, 1210-1218, 2013.